

Spreading and bistability of droplets on differentially heated substrates

J. B. Bostwick[†]

Department of Mathematics, North Carolina State University, Raleigh, NC 27695, USA

(Received 18 July 2012; revised 3 February 2013; accepted 12 April 2013;
first published online 17 May 2013)

An axisymmetric drop spreads on a radially heated, partially wetting solid substrate in a rotating geometry. The lubrication approximation is applied to the field equations for this thin viscous drop to yield an evolution equation that captures the dependence of viscosity, surface tension, gravity, centrifugal forces and thermocapillarity. We study the quasi-static spreading regime, whereby droplet motion is controlled by a constitutive law that relates the contact angle to the contact-line speed. Non-uniform heating of the substrate can generate both vertical and radial temperature gradients along the drop interface, which produce distinct thermocapillary forces and equivalently flows that affect the spreading process. For the non-rotating system, competition between surface chemistry (wetting) and thermocapillary flows induced by the thermal gradients gives rise to bistability in certain regions of parameter space in which the droplets converge to an equilibrium shape. The centrifugal forces that develop in a rotating geometry enlarge the bistability regions. Parameter regimes in which the droplet spreads indefinitely are identified and spreading laws are computed to compare with experimental results from the literature.

Key words: drops and bubbles, interfacial flows (free surface), thermocapillarity

1. Introduction

Manipulation of droplets on the micro-scale is of fundamental interest in industrial applications, primarily because of the advent of microfluidic devices (Stone, Stroock & Ajdari 2004), which often require the interaction between competing physical effects to operate. Surface stresses are particularly useful to drive internal flows in such devices, because of large surface-to-volume ratios (Darhuber & Troian 2005). With regard to droplet spreading, external forces can greatly affect the dynamics: gravitational (Ehrhard & Davis 1991) and centrifugal (Spaid & Homsy 1996) body forces generate pressure gradients in the bulk that drive flow; surface stresses from thermal (Davis 1987) or surfactant concentration (Matar & Craster 2009) gradients induce shear flows; and wettability gradients (Daniel, Chadhury & Chen 2001) generate contact forces and thus contact-line motions. The review article by Oron, Davis & Bankoff (1997) summarizes some of the theoretical work on thin-film flows.

We consider the spreading of an axisymmetric droplet on a differentially heated, partially wetting solid substrate, set in a slowly rotating geometry. Differential heating generates radial thermal gradients in the droplet that, in turn, produce thermocapillary

[†] Email address for correspondence: jbbostwi@ncsu.edu

flows that alter the contact angle and consequently the spreading dynamics. If conductive heat transfer is allowed at the liquid/gas interface, then vertical thermal gradients and their associated thermocapillary flows also develop within the drop. We show that the flow induced by this complex thermal field can compete with the surface chemistry (wetting) giving rise to bistability, whereby there exist two distinct stable equilibrium configurations for one set of system parameters. Bistability is pervasive in fluid mechanics and has been observed in Rayleigh–Bénard convection of an inclined fluid layer (Daniels *et al.* 2008), turbulent rotating spherical Couette flow (Zimmerman, Triana & Lathrop 2011), and the capillary switch (Vogel, Ehrhard & Steen 2005), which is utilized in technologies such as the liquid lens (Lopez & Hirsra 2008) and the switchable capillary adhesion device (Vogel & Steen 2010). With regard to the spreading drop, we identify regions of bistability in a four-dimensional parameter space that characterizes the thermal field, rotation rate and wetting properties. In these regions, the droplet may evolve through a number of intermediate states before reaching its final equilibrium radius. The approach to equilibrium is governed by a dynamic contact-line law relating the contact angle to the contact-line speed.

A droplet of liquid will spread on a solid substrate until it reaches its equilibrium radius, where the balances represented by the Young–Laplace and Young–Dupré equations apply. The former relates the jump in capillary pressure across the fluid interface to the hydrostatic pressure within the drop, whereas the latter constitutes the balance of wetting forces at the contact line or tri-junction between the liquid/gas/solid. During spreading, the fluid motion is largely controlled by the motion of the contact lines. Accordingly, modelling the dynamics of the contact line is of paramount importance, and has been the subject of the large volume of work summarized in the reviews by Dussan V. (1979), de Gennes (1985) and Bonn *et al.* (2009). One prominent feature of the moving contact line is the well-known shear-stress singularity in the flow field that is associated with enforcement of the no-slip condition (Huh & Scriven 1971; Dussan V. 1976). To relieve the stress singularity, one generally allows the fluid to ‘slip’ at the contact line, with the slip modelled according to a variety of proposed functional forms (Huh & Scriven 1971; Dussan V. & Davis 1974; Dussan V. 1976; Ehrhard & Davis 1991; Benintendi & Smith 1999). In addition, one needs to specify a functional form for the contact angle versus contact-line speed relationship, which will be discussed in a subsequent paragraph.

Isothermal spreading of liquid drops has been the subject of a number of studies on moving contact lines. These studies are distinguished by how they treat the dynamics of the contact line. Greenspan (1978) uses the lubrication approximation to derive an evolution equation for a droplet spreading under viscous and capillary forces. Here the evolution equation is coupled to a proposed contact-line law that assumes the contact angle is linearly related to the contact-line speed. Tanner (1979) conducted spreading experiments for planar and axisymmetric silicone oil drops in the capillary-dominated limit to verify a set of proposed spreading laws, which were experimentally confirmed by Chen (1988) for axisymmetric droplets. Ehrhard & Davis (1991) generalize the analysis of Greenspan (1978) to include gravity; their dynamic contact-line model includes a mobility exponent and they report spreading laws in various regimes. As an alternative to the dynamic contact-angle model, Hocking (1983) assumes the instantaneous contact angle is always equal to its static value and is able to reproduce the aforementioned spreading laws from an asymptotic analysis. The choice of the appropriate contact-line model has been a source of dispute in the literature. So much so that Hocking (1992) compared static and dynamic contact-line

models, demonstrating that both models can explain related experiments and arguing that one should apply the simpler static model.

Temperature gradients along fluid interfaces can drive flows via thermocapillarity, whereby surface-tension gradients induce shear stresses, and equivalently flows. The review article by Davis (1987) illustrates the various ways in which an imposed temperature gradient can drive flows, depending upon the orientation of the gradient to the fluid interface. For example, normal gradients can lead to steady Marangoni convection (Pearson 1958) in one-layer systems, whereas tangential gradients can drive steady shear flows and their associated instabilities (Smith & Davis 1983*a,b*). In general, the imposed temperature gradient will involve some combination of both normal and tangential gradients if the interface is curved, as is true for droplets.

Ehrhard & Davis (1991) consider the spreading of two-dimensional and axisymmetric drops on uniformly heated (cooled) substrate. Under such heating (cooling), a vertical temperature gradient is established within the drop if the fluid is non-thermally simple or can conduct heat across the interface. For reference, a thermally simple fluid is characterized by a uniform temperature field within the fluid domain and the absence of heat transfer. The thermocapillary flow induced by this heating consists of a recirculation cell that alters the contact angle in a manner that inhibits (assists) spreading, if the substrate is uniformly heated (cooled). Ehrhard (1993) verifies these results experimentally, while Ehrhard (1994) extends the analysis to include pendant drops. In a similar study, Dunn *et al.* (2009) derive an implicit solution to the quasi-static evolution equation for a two-dimensional ridge on a uniformly heated (cooled) substrate showing that there may exist up to three unique stable equilibrium configurations, depending upon the heating.

Darhuber, Troian & Wagner (2002) demonstrate that high-resolution substrate temperature distributions can be achieved via embedded microheaters, which can, in turn, generate horizontal temperature gradients in thin films and droplets. With regard to droplets, the asymmetric Marangoni stresses induced by these thermal gradients can lead to droplet migration, provided that ‘pinning’ effects from contact-angle hysteresis can be overcome (Chen *et al.* 2005). Ford & Nadim (1994) were able to derive an expression for the migration speed of a two-dimensional ridge that depends upon the interface shape, contact-angle hysteresis interval and Navier slip coefficient. Smith (1995) utilizes the lubrication approximation to study the response of a two-dimensional droplet subject to a linear substrate temperature distribution, while also allowing for conductive heat transfer across the droplet interface. The resulting temperature profile produces a thermocapillary recirculation cell that affects the contact-line dynamics leading to steady-state droplet migration at a constant speed. The vast majority of work on the thermal actuation of droplets, as summarized in the review article by Darhuber & Troian (2005), is concerned with liquids on partially wetting (hydrophilic) substrates so that the lubrication approximation is applicable. More recently, Nguyen & Chen (2010*b*) have studied thermocapillary migration of two-dimensional drops using the finite-element method to show that the migration speed of droplets is larger on hydrophobic substrates than on hydrophilic ones. If these droplets are large enough, buoyancy-driven convection becomes important and can significantly slow the speed of droplet migration (Nguyen & Chen 2010*a*).

In contrast to the differential heating described above, Mukhopadhyay & Behringer (2009) study droplet spreading using an experimental apparatus that can generate non-uniform radial temperature gradients on a partially wetting solid substrate in a rotating geometry. Their apparatus is novel in the sense that non-uniform thermal gradients can be generated that are also symmetric about the axis-of-rotation. Mukhopadhyay

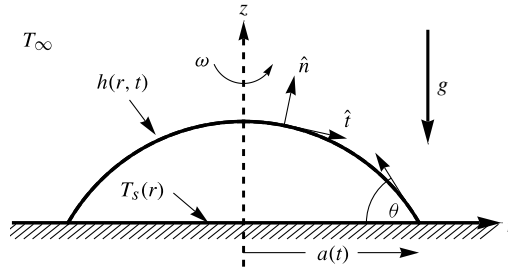


FIGURE 1. Definition sketch of the spreading droplet.

& Behringer (2009) demonstrate that a droplet on a completely wetting substrate can be made to retract to a smaller equilibrium radius under a strong thermal gradient. Our results confirm this observation and yield a prediction that relates the equilibrium radius to the magnitude of the thermal gradient. They measure the time-dependent contact angle throughout the retraction process and report power-law behaviour with an uncharacteristic spreading exponent. We recover this power-law behaviour from our analysis in the appropriate limit. The apparatus used in these experiments can generate a number of mechanisms that cause the droplet to either spread or retract, such as pressure gradients from gravitational and centrifugal (body) forces, shear stresses via thermocapillarity (surface) or wetting (contact) forces. A goal of this work is to analyse the interactions amongst these various spreading mechanisms and how this coupling alters the spreading process.

In the sections that follow, the governing equations are formulated and the lubrication approximation is applied to yield an evolution equation for the droplet shape. For small spreading rates, the droplet shape is steady and evolves according to a dynamic contact-line condition that describes the motion of the contact line and therefore the bulk droplet motion. An asymptotic solution is constructed for small heating and two external heating conditions. Our results focus on equilibrium states and their stability, the approach to equilibrium via the dynamic contact-line law and the flows induced by the thermal field. The parameter space is mapped to identify regions of bistability and indefinite spreading. Finally, some concluding remarks are offered.

2. Mathematical formulation

Consider a liquid droplet on a smooth, non-uniformly heated, horizontal substrate that is rotating at a constant angular velocity ω about the vertical axis in axisymmetric cylindrical coordinates (r, z) , as shown in figure 1. The droplet of an incompressible Newtonian fluid with density ρ , dynamic viscosity μ , specific heat c_p and thermal conductivity k , is immersed in a passive gas of temperature T_∞ that conductively heats or cools the droplet. The liquid and gas phases are separated by an interface $z = h(r, t)$ that is defined on the domain between the axis-of-symmetry ($r = 0$) and the three-phase moving contact line $r = a(t)$.

2.1. Field equations

To describe the motion of the fluid, we introduce the velocity $\mathbf{v} = (u, w)$, pressure p and temperature T fields. The velocity field satisfies the continuity equation,

$$\nabla \cdot \mathbf{v} = 0, \tag{2.1}$$

as required by incompressibility. A balance of linear momentum on a material volume results in the Navier–Stokes equation,

$$\rho \left(\frac{\partial \mathbf{v}}{\partial t} + \mathbf{v} \cdot \nabla \mathbf{v} \right) = \mu \nabla^2 \mathbf{v} - \nabla p - \rho g \hat{\mathbf{z}} + \rho \omega^2 r \hat{\mathbf{r}}, \quad (2.2)$$

where g is magnitude of the gravitational acceleration, $\hat{\mathbf{r}} = (1, 0)$ is the radial unit vector and $\hat{\mathbf{z}} = (0, 1)$ is the vertical unit vector. Similarly, the balance of thermal energy gives

$$\rho c_p \left(\frac{\partial T}{\partial t} + \mathbf{v} \cdot \nabla T \right) = k \nabla^2 T. \quad (2.3)$$

2.2. Boundary conditions

The fluid is bounded from below by a rigid, flat, perfectly conducting substrate $z = 0$, where the no-penetration, Navier-slip and time-independent temperature distribution conditions are enforced, respectively:

$$w = 0, \quad v = \beta' \frac{\partial v}{\partial z}, \quad T = T_s(r) \equiv T_0 + T_n(r). \quad (2.4)$$

Here the slip coefficient β' is a small number that is introduced to relieve the shear-stress singularity at the contact line (Dussan V. & Davis 1974). In addition, it will be assumed that the applied temperature distribution $T_s(r)$ can be decomposed as the sum of a constant reference temperature T_0 and a radially dependent temperature $T_n(r)$ that generates a monotonic temperature gradient.

Similarly, the free surface $z = h(r, t)$ (liquid/gas interface) bounds the fluid from above and one applies the requisite kinematic condition, balance of normal and shear stresses, and a mixed thermal boundary condition there:

$$h_t + v h_r = w, \quad \hat{\mathbf{n}} \cdot \mathbf{T} \cdot \hat{\mathbf{n}} = -\sigma (2H), \quad \hat{\mathbf{t}} \cdot \mathbf{T} \cdot \hat{\mathbf{n}} = \hat{\mathbf{t}} \cdot \nabla \sigma, \quad k \nabla T \cdot \hat{\mathbf{n}} = -h_g (T - T_\infty). \quad (2.5)$$

Here \mathbf{T} is the stress tensor, σ is the liquid–gas surface tension, h_g is the heat transfer coefficient and subscripts on the free-surface shape $h(r, t)$ denote partial differentiation with respect to the variables r and t . The mixed thermal boundary condition is used to allow for the possibility of conduction-dominated heat transfer across the free surface. The unit vectors normal $\hat{\mathbf{n}}$ and tangent $\hat{\mathbf{t}}$ to the free surface $h(r, t)$ are defined as

$$\hat{\mathbf{n}} = (-h_r, 1) / \sqrt{1 + h_r^2}, \quad \hat{\mathbf{t}} = (1, h_r) / \sqrt{1 + h_r^2}, \quad (2.6)$$

while the curvature of that surface is given by

$$2H = - \left(h_{rr} + \frac{1}{r} h_r \right). \quad (2.7)$$

The thermocapillary effect is modelled by assuming an equation of state for the surface tension $\sigma = \sigma(T)$ that depends linearly upon the temperature

$$\sigma = \sigma_0 - \gamma (T - T_0), \quad (2.8)$$

where $\gamma = -d\sigma/dT > 0$ is the rate of change of surface tension with respect to temperature, T_0 is the previously mentioned reference temperature and σ_0 is the surface tension at that reference temperature.

The contact line $r = a(t)$ is located at the intersection of the solid substrate and free surface, or the tri-junction of the solid/liquid/gas phases (cf. figure 1). Here

$$h(a(t), t) = 0, \tag{2.9}$$

and the contact angle $\theta(t)$ is defined by the geometric relationship,

$$\frac{\partial h}{\partial r}(a(t), t) = -\tan \theta(t). \tag{2.10}$$

At the contact line, kinematics requires the fluid velocity to equal the contact-line velocity $u_{CL} \equiv v(a(t), t) = da/dt$, which is modelled using a constitutive relationship that relates the contact-line speed to the contact angle (cf. Ehrhard & Davis 1991),

$$\frac{da}{dt} = \kappa(\theta - \theta_A)^m, \tag{2.11}$$

where $\kappa > 0$ is an empirical constant, $\theta_A \geq 0$ is the advancing (static) contact angle, and m is a spreading exponent that is typically 1 (Greenspan 1978) or 3 (Tanner 1979).

To ensure the drop shape remains axisymmetric throughout the spreading process, the following conditions are imposed on the axis-of-symmetry ($r = 0$):

$$h_r|_{r=0} = 0, \quad h_{rrr}|_{r=0} = 0. \tag{2.12}$$

Finally, we enforce conservation of the droplet volume V_0 ,

$$2\pi \int_0^{a(t)} rh(r, t) dr = V_0. \tag{2.13}$$

2.3. Scalings

The following dimensionless variables are introduced:

$$\left. \begin{aligned} \tilde{r} &= \frac{r}{a_0}, & \tilde{z} &= \frac{z}{a_0\theta_0}, & \tilde{t} &= \frac{\sigma_0}{a_0\theta_0\mu}t, & \tilde{w} &= \frac{\mu}{\sigma_0}w, & \tilde{v} &= \frac{\mu}{\sigma_0\theta_0}v, \\ \tilde{p} &= \frac{a_0}{\sigma_0\theta_0}p, & \tilde{T} &= \frac{T - T_\infty}{T_0 - T_\infty}, & \tilde{\theta} &= \frac{\theta}{\theta_0}, & V &= \frac{V_0}{a_0^3\theta_0}. \end{aligned} \right\} \tag{2.14}$$

Here the initial droplet shape is used to scale the spatial variables (r, z). We use a viscous velocity scale and scale the pressure with the capillary pressure. The temperature is scaled with respect to the difference between the reference and ambient temperatures, $T_0 - T_\infty$.

The scalings (2.14) are applied to the governing equations (2.1)–(2.13) which can then be expanded in terms of the initial contact angle θ_0 , taken to be a small parameter. The leading-order expansion (lubrication approximation) gives a reduced set of field equations,

$$\frac{1}{r}(rv)_r + w_z = 0, \quad -p_r + w_{zz} + \Omega^2 r = 0, \quad -p_z - G = 0, \quad T_{zz} = 0, \tag{2.15}$$

where subscripts denote differentiation and the tildes have been dropped for simplicity. The relevant boundary conditions on the substrate $z = 0$ are given by

$$v = \beta v_z, \quad w = 0, \quad T = 1 - NT_n(r), \tag{2.16}$$

where N is a dimensionless parameter used to measure the strength of the applied temperature distribution. Similarly, the reduced free-surface boundary conditions

on $z = h(r, t)$ are written as

$$h_t + vh_r = w, \quad -p = h_{rr} + \frac{1}{r}h_r, \quad \Delta C v_z = -(T_r + h_r T_z), \quad T_z + BT = 0. \quad (2.17)$$

The dynamic contact-line condition is given by

$$\frac{da}{dt} = \mathcal{K}(\theta - \theta_A)^m. \quad (2.18)$$

The dimensionless groups that result from this choice of scaling are given by

$$\left. \begin{aligned} G &= \frac{\rho g a_0^2}{\sigma_0}, & \Omega^2 &= \frac{\rho \omega^2 a_0^3}{\sigma_0 \theta_0}, & \beta &= \frac{\beta'}{a_0 \theta_0}, & \Delta C &= \frac{\sigma_0}{\gamma (T_0 - T_\infty) \theta_0^2}, \\ B &= \frac{h_g a_0 \theta_0}{k}, & \mathcal{K} &= \frac{\kappa \theta_0^{m+1} \mu}{\sigma} \end{aligned} \right\} \quad (2.19)$$

which are the Bond number G , centrifugal number Ω^2 , slip number β , thermocapillary number ΔC and Biot number B . The parameter \mathcal{K} is a measure of the contact-line (wettability) velocity, and the dimensionless radial temperature gradient N is set by the applied temperature field, to be given subsequently.

2.4. Derivation of evolution equation

To derive the evolution equation, one begins by constructing a solution to the governing equations (2.15)–(2.17) that depends implicitly on the free-surface shape h . Then, the evolution equation is generated from a depth-averaged continuity equation

$$h_t + (1/r)(rq)_r = 0, \quad (2.20)$$

where q is the net radial flux in the droplet, computed by integrating the radial velocity over the liquid layer.

The temperature field inside the droplet satisfies the reduced energy equation (2.15), subject to boundary conditions on the substrate (2.16) and free surface (2.17),

$$T = (1 - N T_n(r)) \left(\frac{1 + B(h - z)}{1 + Bh} \right). \quad (2.21)$$

Similarly, the pressure is computed from the vertical component of the Navier–Stokes equations (2.15) and normal stress balance on the free surface (2.17),

$$p = G(h - z) - \left(h_{rr} + \frac{1}{r}h_r \right). \quad (2.22)$$

The radial velocity field is calculated from the radial component of the Navier–Stokes equations (2.15), Navier-slip condition (2.16) and tangential stress balance (2.17),

$$v = (p_r - \Omega^2 r) \left(\frac{1}{2}z^2 - (z + \beta)h \right) + S(z + \beta) \quad (2.23)$$

where the pressure is given by (2.22) and

$$S \equiv -\frac{1}{\Delta C} (T_r + h_r T_z) = \frac{1}{\Delta C} \left(N \frac{(T_n)_r}{1 + Bh} + B \frac{h_r (1 - N T_n)}{(1 + Bh)^2} \right). \quad (2.24)$$

Here, the temperature is defined in (2.21). Finally, one uses the reduced continuity equation (2.15) and no-penetration condition (2.16) to compute the vertical velocity,

$$w = - \left(p_{rr} + \frac{1}{r} p_r - 2\Omega^2 \right) \left(\frac{1}{6} z^3 - h \left(\frac{1}{2} z^2 + \beta z \right) \right) - \left(S_r + \frac{S}{r} \right) \left(\frac{1}{2} z^2 + \beta z \right), \quad (2.25)$$

with p and S defined in (2.22) and (2.24), respectively.

The flow generated by the fields defined in (2.21)–(2.25) are applied to the depth-averaged continuity equation (2.20) to generate the evolution equation,

$$h_t + \frac{1}{r} \left(r \left(\left(h_{rr} + \frac{1}{r} h_r - Gh \right)_r + \Omega^2 r \right) \left(\frac{1}{3} h^3 + \beta h^2 \right) + r \left(\frac{N}{\Delta C} \frac{(T_n)_r}{1 + Bh} + \frac{B}{\Delta C} \frac{h_r (1 - NT_n)}{(1 + Bh)^2} \right) \left(\frac{1}{2} h^2 + \beta h \right) \right) = 0. \quad (2.26)$$

The droplet shape and its motion along the solid substrate are governed by the evolution equation (2.26), the dimensionless form of the contact-line conditions (2.9)–(2.11) and conservation of volume constraint (2.13). Once the free-surface shape h is known, the temperature, pressure and velocity fields are then computed from (2.21)–(2.25).

2.5. Quasi-static spreading

A number of assumptions are implemented to facilitate a solution of the evolution equation (2.26) that focus on qualitative aspects of the various physical mechanisms that govern the spreading process. For purposes of clarity each assumption will be motivated and the modelling implications will be expounded upon.

Spreading rates can be of the order of microns per second, which is typically much slower than the velocity scale obtained by balancing viscosity with surface tension. Under such conditions, $h_t = 0$ and the evolution equation (2.26) describes a steady droplet shape that is parameterized by the contact-line radius, which evolves according to the dynamic contact-line condition (2.18). More precisely, the free-surface shape evolves implicitly through the time-dependent contact-line radius. This motion is deemed quasi-static and has been analysed in a similar context by a number of authors (e.g. Rosenblat & Davis 1985; Ehrhard & Davis 1991; Smith 1995). As noted in these studies, the leading-order problem consists of a steady droplet shape with no contact-line motion. Accordingly, the shear-stress singularity associated with a moving contact line is absent and, therefore, we set the slip number $\beta = 0$.

Two final assumptions are made with respect to the thermal properties of the fluid and the applied thermal gradient. First, the Biot number is assumed to be small $B \ll 1$, which is plausible for small droplets and/or thermally simple fluids. Recall that a thermally simple fluid cannot conduct heat across its interface. Second, the magnitude of the applied thermal gradient is small, $NT_n \ll 1$. Although they appear independent, Smith (1995) noted that the latter assumption is redundant with respect to the former if the temperature gradient applied to the solid substrate is also applied to the gas above the droplet. Note that this restriction is on the temperature gradient, so that the respective temperature profiles can vary by a constant temperature. Under these heating conditions, there is no restriction on the applied thermal gradient.

The assumptions are applied to the evolution equation (2.26), which is then integrated to yield an equation governing the steady droplet shape,

$$\left(h_{rr} + \frac{1}{r} h_r - Gh \right)_r + \Omega^2 r + \frac{3}{2} \frac{1}{h} (\hat{N} (T_n)_r + \hat{M} h_r) = 0. \quad (2.27)$$

The integration constant is set to zero by conservation of mass and the thermal Marangoni numbers are defined as

$$\hat{N} \equiv \frac{N}{\Delta C}, \quad \hat{M} \equiv \frac{B}{\Delta C}. \tag{2.28}$$

Here \hat{N} is representative of the radial gradient that develops within the fluid because of the applied temperature distribution on the solid substrate, whereas \hat{M} characterizes the vertical gradient that results from heat transfer across the free surface (cf. (2.21)).

3. Solution method

The parameter space for this problem is large ($\hat{M}, \hat{N}, \Omega^2, G, \theta_A, m$) and the applied temperature distribution T_n can take an infinity of forms. Therefore, we consider a smaller subset of parameters to more tightly focus the scope of the results presented here. To that end, we suppress the role of gravity by setting $G = 0$, and consider both linear and logarithmic applied temperature distributions (Mukhopadhyay & Behringer 2009). An asymptotic solution for the droplet shape is constructed from (2.27) using a regular perturbation expansion for small Ω^2 , \hat{M} and \hat{N} to illustrate how the interface shape changes locally near the contact line with the system parameters. The assumption of small Marangoni numbers \hat{M}, \hat{N} is reasonable, while the centrifugal number Ω^2 need not be small in practice, but is taken to be small to clarify some of the qualitative aspects of this study. Finally, the asymptotic solution is then mapped to the contact-line condition

$$\frac{da}{dt} = \mathcal{K}(-h_r(a) - \theta_A)^m, \tag{3.1}$$

which governs the rate of spreading.

3.1. Linear temperature distribution

The first temperature distribution we consider has a linear profile

$$T_n = r, \quad N = \frac{ba_0}{T_0 - T_\infty}. \tag{3.2}$$

Here one should recall that a constant temperature has been absorbed into the definition of the applied thermal distribution so that the radial gradient is generated solely by T_n and the convention is that the gradient is directed from the axis-of-symmetry (hot) to the contact line (cold) for $\hat{N} > 0$. We compute the asymptotic solution from (2.27),

$$\begin{aligned} h(r) = & \frac{2}{\pi a^4} (a^2 - r^2) + \frac{\Omega^2}{32} (a^2 - r^2) (r^2 - a^2/3) \\ & + \hat{M} \left(\frac{9}{16} (r^2 - a^2) + \frac{\pi^2 a^2}{16} + \frac{3}{8} (a^2 - r^2) \ln(1 - (r/a)^2) - \frac{3}{8} Li_2((r/a)^2) \right) \\ & + \hat{N} \left(\frac{\pi a^3}{64} (a^2 (28 - 3\pi^2) - 36ar + 8r^2 + 12(a^2 - r^2) \tanh^{-1}(r/a) \right. \\ & \left. + 6a^2 (4Li_2(r/a) - Li_2((r/a)^2))) \right), \end{aligned} \tag{3.3}$$

where Li_2 is the dilogarithm function. Finally, we apply the asymptotic solution to the dynamic contact-line condition (3.1) to yield

$$\frac{da}{dt} = \mathcal{K} \left(\frac{4}{\pi a^3} - \hat{M} \left(\frac{3}{8} \right) a + \Omega^2 \left(\frac{1}{24} \right) a^3 + \hat{N} \left(\frac{\pi}{8} \right) a^4 - \theta_A \right)^m. \quad (3.4)$$

3.2. Logarithmic temperature distribution

The experimental apparatus used by Mukhopadhyay & Behringer (2009) to differentially heat their solid substrate can be idealized as an annulus with small aspect ratio, subject to prescribed temperatures on the inner and outer surfaces. The temperature distribution for this type of heating is governed by Laplace’s equation in axisymmetric cylindrical coordinates with Dirichlet boundary conditions and has a well-known logarithmic profile,

$$T_n = \ln r, \quad N = \frac{b}{T_0 - T_\infty}. \quad (3.5)$$

We compute the asymptotic solution from (2.27),

$$\begin{aligned} h(r) = & \frac{2}{\pi a^4} (a^2 - r^2) + \frac{\Omega^2}{32} (a^2 - r^2) (r^2 - a^2/3) \\ & + \hat{M} \left(\frac{9}{16} (r^2 - a^2) + \frac{\pi^2 a^2}{16} + \frac{3}{8} (a^2 - r^2) \ln (1 - (r/a)^2) - \frac{3}{8} Li_2 ((r/a)^2) \right) \\ & + \hat{N} \left(\frac{1}{64} (-\pi^3 a^4 + 6\pi a^2 (2 \ln a - 1) (r^2 - a^2) + 6\pi a^2 (a^2 \ln a - r^2 \ln r) \right. \\ & \left. + (r^2 - a^2) \ln (1 - (r/a)^2) + 6\pi a^4 Li_2 ((r/a)^2) \right), \end{aligned} \quad (3.6)$$

which is then substituted into the dynamic contact-line condition (3.1) resulting in

$$\frac{da}{dt} = \mathcal{K} \left(\frac{4}{\pi a^3} - \hat{M} \left(\frac{3}{8} \right) a + C_{\hat{N}\Omega} a^3 - \theta_A \right)^m. \quad (3.7)$$

The parameter $C_{\hat{N}\Omega}$ combines the effect of radial thermal gradients and centrifugal forces,

$$C_{\hat{N}\Omega} \equiv \frac{\Omega^2}{24} + \hat{N} \left(\frac{3\pi}{16} \right). \quad (3.8)$$

4. Results

The results presented here will focus on equilibrium states and their stability and the approach to equilibrium via the dynamic contact-line condition. We begin by describing the thermocapillary flows induced by the vertical ($\hat{M} \neq 0, \hat{N} = 0$) and radial ($\hat{N} \neq 0, \hat{M} = 0$) thermal gradients. For the more general heating condition $\hat{M} \neq 0, \hat{N} \neq 0$, the flow induced by the thermal field can compete with the surface chemistry (wetting) giving rise to bistability, whereby two stable equilibrium configurations exist for one set of system parameters. The parameter regimes where bistability occurs are identified for two typical heating conditions, as well as regions where the droplet spreads indefinitely.

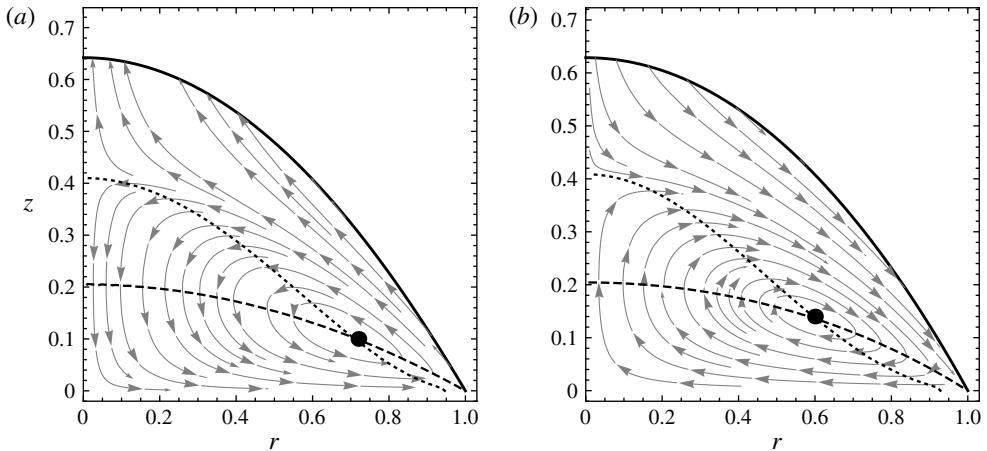


FIGURE 2. Streamlines for a droplet spreading by a strictly (a) vertical ($\hat{M} = 0.1, \hat{N} = 0$) and (b) radial ($\hat{M} = 0, \hat{N} = 0.1$) thermal gradient showing stagnation points and curves of zero radial (dashed) and vertical (dotted) velocity.

4.1. Thermocapillary flows

We compare the thermocapillary flows induced by the vertical and radial thermal gradient and their effect on the spreading process. For clarity, we set the rotation rate $\Omega^2 = 0$ and consider the linear applied temperature distribution (3.2). Here one should recall the convention is that a positive radial Marangoni number $\hat{N} > 0$ denotes a radial temperature gradient directed from the axis-of-symmetry (hot) to the contact line (cold), whereas the vertical Marangoni number $\hat{M} > 0$ is positive if the reference temperature of the substrate (hot) is larger than the ambient temperature (cold).

Ehrhard & Davis (1991) studied the case of uniform heating or cooling of the solid substrate ($\hat{M} \neq 0, \hat{N} = 0$). They show that heating the substrate, $\hat{M} > 0$, generates a temperature profile that decreases along the drop interface from the contact line to the axis-of-symmetry which, in turn, produces a thermocapillary recirculation cell, as shown in figure 2(a). The counterclockwise-rotating recirculation cell is a consequence of mass conservation, whereby the flow generated along the interface from the surface-tension gradient is redirected back along the solid substrate. This flow inhibits spreading by decreasing the contact angle and therefore the contact-line speed via (3.1). The converse is true for a cooling substrate, $\hat{M} < 0$. For a radial thermal gradient oriented in the positive sense, $\hat{N} > 0$, there is a surface flow from the axis-of-symmetry (hot) to the contact line (cold), which is then redirected back along the solid substrate towards the axis-of-symmetry generating a clockwise-rotating recirculation cell, as shown in figure 2(b). This type of flow assists spreading. In contrast, reversing the orientation of the radial gradient, $\hat{N} < 0$, tends to inhibit spreading. Smith (1995) has reported a recirculation cell of the latter type for two-dimensional drops that aids droplet migration. The assumption of axisymmetry precludes this type of motion and both types of recirculation cell exist in symmetric pairs that can either assist or inhibit spreading.

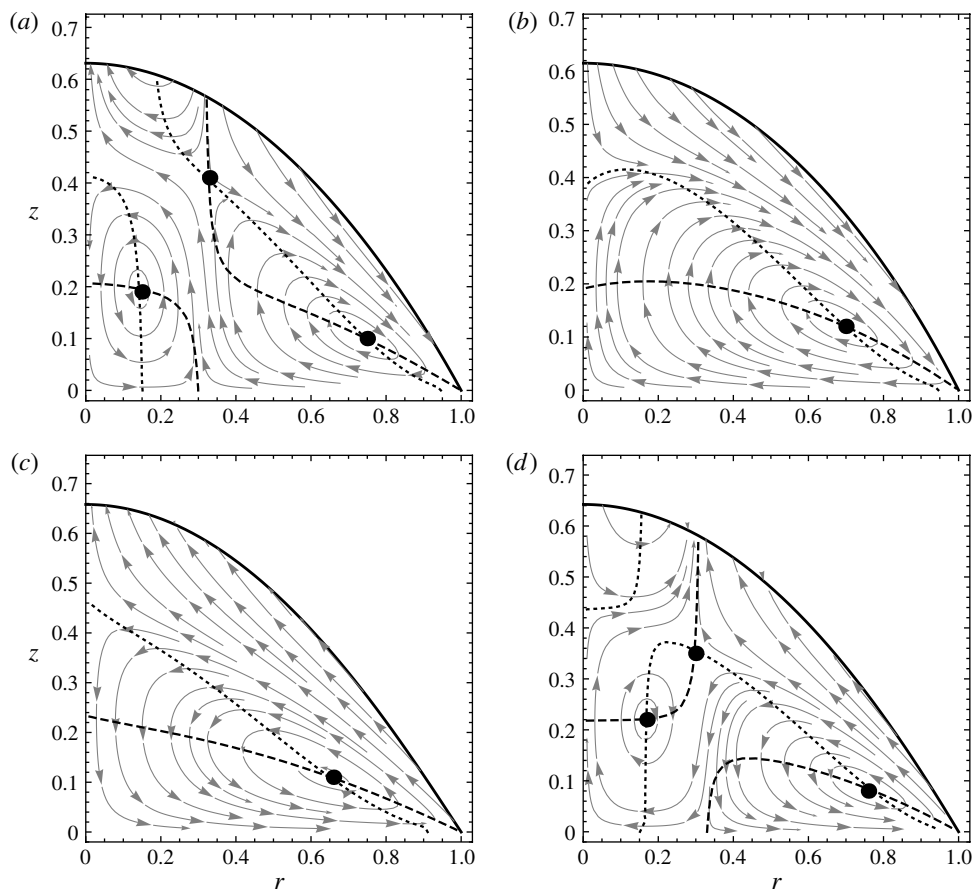


FIGURE 3. Streamlines for a droplet spreading under a thermal gradient characterized by Marangoni numbers (a) $\hat{M} = -0.25$, $\hat{N} = -0.1$, (b) $\hat{M} = -0.25$, $\hat{N} = 0.1$, (c) $\hat{M} = 0.25$, $\hat{N} = 0.1$ and (d) $\hat{M} = 0.25$, $\hat{N} = 0.1$, showing stagnation points and curves of zero radial (dashed) and vertical (dotted) velocity.

4.2. Bistability

For general heating conditions, the drop will attain a complex temperature profile that generates both vertical and radial gradients along the drop interface. The flows induced by these thermocapillary forces can either work in concert or competition to alter the contact angle and therefore the spreading process through the contact-line dynamics. Figure 3 shows prototypical flows for the various sub-cases. If the thermocapillary forces act in concert, the two effects combine to form a single recirculation cell rotating in the direction consistent with assisted (clockwise) or inhibited (counter-clockwise) spreading (cf. figure 3*b,c*). On the contrary, a set of localized recirculation cells exist when the corresponding thermocapillary forces are in competition (cf. figure 3*a,d*). These localized recirculation cells evolve and interact throughout the spreading process.

Thermocapillary flows can alter the contact angle and therefore the balance of forces at the contact line (3.4), which is an ordinary differential equation of the form $da/dt = f(a)$. We compute the equilibrium radius a_∞ by setting the contact-line

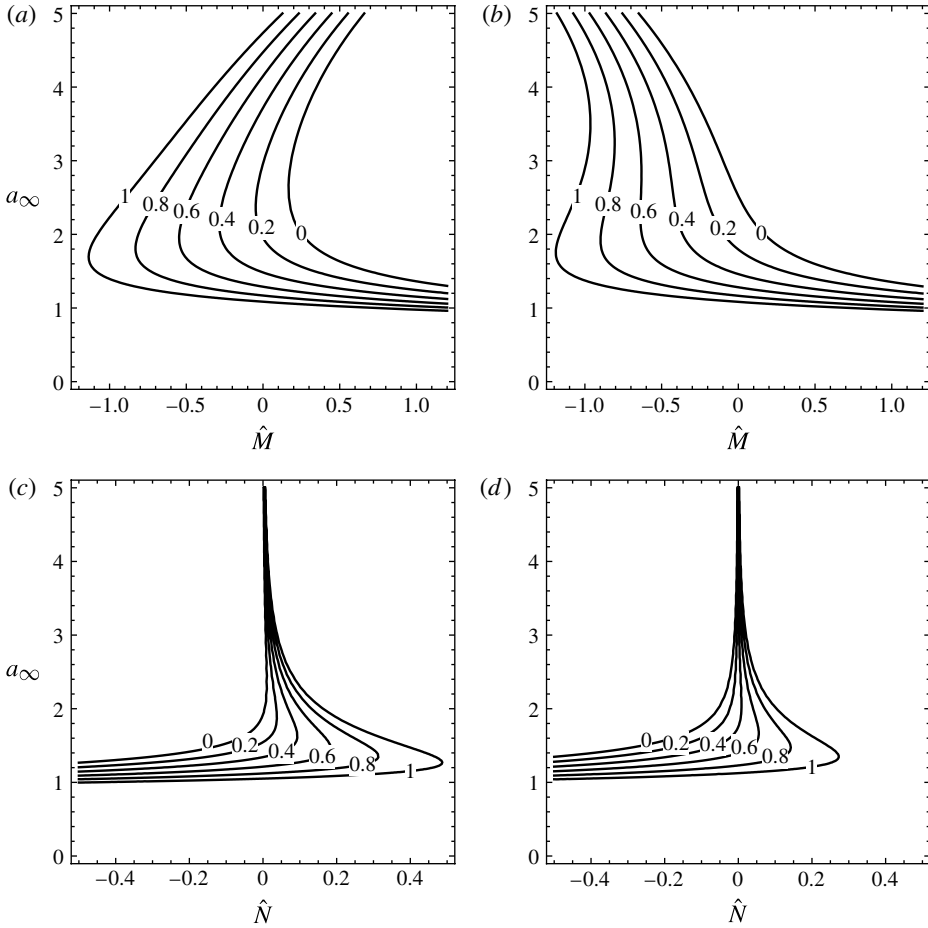


FIGURE 4. Bifurcation diagram: equilibrium radius a_∞ against (a,b) vertical Marangoni number \hat{M} , for fixed (a) $\hat{N} = 0.005$ and (b) $\hat{N} = -0.005$, and (c,d) radial Marangoni number \hat{N} , for fixed (c) $\hat{M} = 0.25$ and (d) $\hat{M} = -0.25$, showing contours of static-contact angle θ_A for $\Omega^2 = 0$.

velocity to zero, $da/dt = 0$, and solving $f(a_\infty) = 0$. Figure 4 plots the equilibrium radius a_∞ as it depends upon the Marangoni numbers \hat{M}, \hat{N} for the non-rotating $\Omega^2 = 0$ geometry. Here figures 4(a), 4(c) and 4(d) are qualitatively similar in that there are regions of parameter space with zero, one or two equilibria, depending upon the wetting conditions θ_A . However, figure 4(b) exhibits regions of three equilibria and is thus qualitatively dissimilar from the other sub-cases. Figure 5 traverses the parameter space (figure 4b) in the direction of decreasing vertical Marangoni number \hat{M} , while holding all other parameters fixed, to illustrate the change in both number and type of equilibria. As the bifurcation diagram is traversed, the number of equilibria changes from one (figure 5a) to three (figure 5c) at the bifurcation point (BP) shown in figure 5(b) and back again from three (figure 5c) to one (figure 5e) at the second bifurcation point (figure 5d). The region of parameter space that lies between the two bifurcation points is a region of bistability, whereby there are two stable equilibria for one set of parameters.

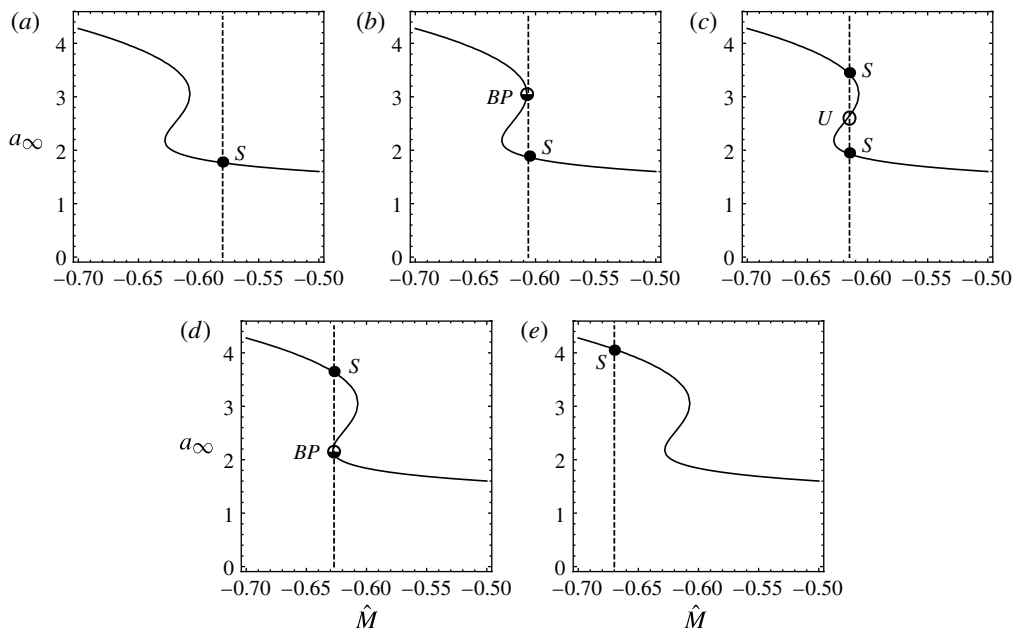


FIGURE 5. Traversing the bifurcation diagram for a fixed radial gradient $\hat{N} = -0.0041$ and static contact angle $\theta_A = 0.6$, while changing the vertical Marangoni number \hat{M} to show bifurcation points (BP) in (b,d) and bistability in (c). Here points S and U denote stable and unstable equilibria, respectively.

Stability of the equilibria mentioned above is deduced by using standard techniques in one-dimensional bifurcation theory that can be applied to (3.4), such as plotting the vector field $f(a)$ to determine the direction of contact-line motion and hence the stability of an equilibrium a_∞ . In addition, one can define a Lyapunov function E , $-dE/da = f(a)$, for the vector field $f(a)$ to visualize the energy landscape around the respective equilibria. Figure 6 plots the bifurcation diagram, vector field and Lyapunov function in the bistability region of figure 5(c). Here one uses the vector field to deduce if the equilibrium is stable (S) or unstable (U), as shown in figure 6(b). The characteristic feature of the bistability region is the Lyapunov function with a double-well potential (cf. figure 6c). Figure 7 plots the equilibrium interface shapes, which are computed numerically from (2.27), in the bistability region shown in figure 6.

The approach to equilibrium in the bistability region of figure 6(a) is governed by the dynamic contact-line condition (3.4). Typically, no characteristic power law can be identified for general heating conditions (cf. figure 8a). In addition, figure 8(b) shows the case where the thermal gradients induce thermocapillary flows which act together. Here two unique retraction rates are visible; the first regime, $t \in [0.01, 1]$, is more film-like and dominated by the radial gradient, while the second regime, $t \in [1, 10]$ is drop-like with a faster retraction rate controlled by the vertical gradient induced by large changes in height along the drop interface.

4.3. Parameter space for linear heating

The results mentioned above illustrate various aspects of the problem considered here, such as spreading power laws, bistability and the approach to equilibrium. Some of these properties are generic and exist for a wide range of system parameters, such as

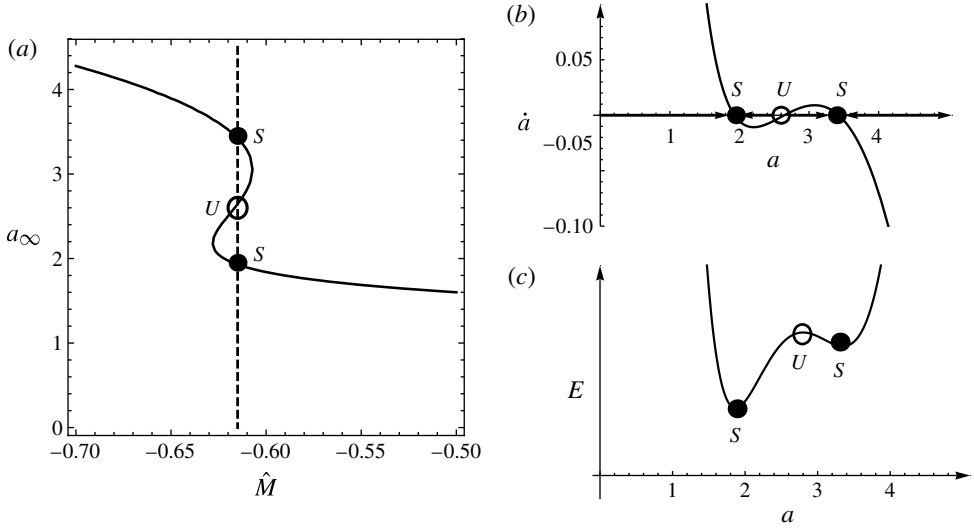


FIGURE 6. Bistability region of figure 5(c): (a) bifurcation diagram plotting the equilibrium radius a_∞ against vertical Marangoni number \hat{M} , (b) vector field \dot{a} and (c) Lyapunov function E against contact-line radius a , for radial Marangoni number $\hat{N} = -0.0041$ and static contact angle $\theta_A = 0.6$.

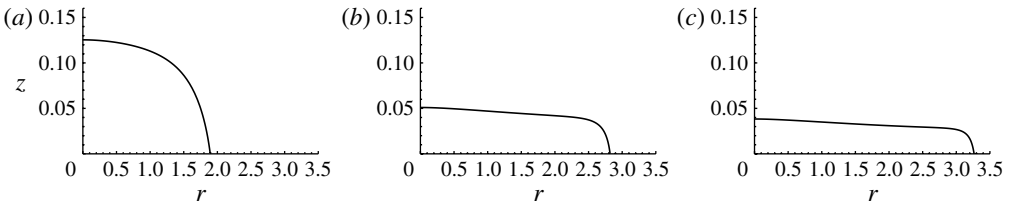


FIGURE 7. Equilibrium interface shapes for the bistability region shown in figure 6 computed numerically from (2.27) with $\hat{N} = -0.0041$, $\hat{M} = -0.61$, $\theta_A = 0.6$, $\Omega^2 = 0$ and contact-line radius (a) $a = 1.8934$, (b) $a = 2.8191$ (c) $a = 3.2809$.

regions of bistability or indefinite spreading, which we define as regions of parameter space without an equilibrium solution. For many coating processes, it is particularly useful to identify parameter regimes where indefinite spreading occurs. The most efficient way to describe the equilibrium states and their dependence on parameters is to take ‘slices’ of the large parameter space $(\hat{M}, \hat{N}, \Omega^2, \theta_A)$.

Descartes’ rule of signs can be used as a guide in identifying the parameter regimes where bistability may or may not occur. The rule states that the number of positive roots of a real-valued polynomial, in order of descending exponents, is either equal to the number of sign changes between consecutive non-zero coefficients or less than it by a multiple of two. For linear heating, the equilibrium equation is given by

$$\hat{N} \left(\frac{\pi}{8}\right) a^4 + \Omega^2 \left(\frac{1}{24}\right) a^3 - \hat{M} \left(\frac{3}{8}\right) a - \theta_A + \frac{4}{\pi a^3} = 0, \tag{4.1}$$

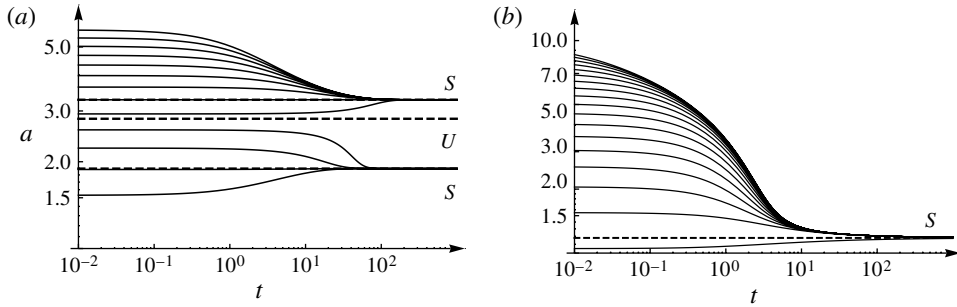


FIGURE 8. Contact-line radius a against time t for (a) the bistability region of figure 5(c) ($\hat{N} = -0.0041, \hat{M} = -0.61, \theta_A = 0.6$) and (b) heating conditions in which the vertical and radial Marangoni forces act in concert ($\hat{M} = 0.3, \hat{N} = -0.001, \theta_A = 0.35$) to illustrate different spreading rates. Here the spreading exponent $m = 1$.

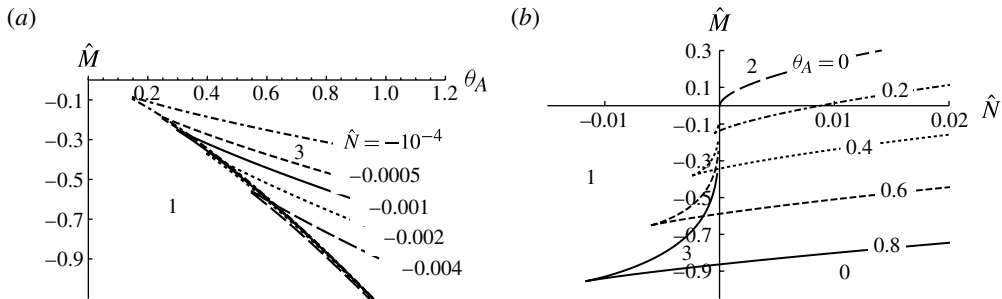


FIGURE 9. Parameter space for linear heating: vertical Marangoni number \hat{M} against (a) radial Marangoni number \hat{N} , parameterized by static contact angle θ_A and (b) θ_A , as it depends upon \hat{N} , for $\Omega^2 = 0$ emphasizing regions of bistability.

where the static contact angle is a positive constant $\theta_A \geq 0$ and the Marangoni numbers \hat{M}, \hat{N} can take either positive or negative values. For no rotation, $\Omega^2 = 0$, a necessary condition for bistability is that the applied radial gradient be directed inward, $\hat{N} < 0$, while the substrate is uniformly cooled, $\hat{M} < 0$. Here one should note that the converse, $\hat{N} > 0, \hat{M} > 0$, does not yield bistability despite producing competing thermocapillary flows from the respective thermal gradients.

Figure 9 plots regions of indefinite spreading and bistability in the non-rotating $\Omega^2 = 0$ subspace, as they depend upon \hat{M}, \hat{N} and θ_A . Figure 9(a) informs one how to choose the appropriate substrate (θ_A) and liquid/reference substrate temperature (\hat{M}) to achieve bistability for a given radial thermal gradient (\hat{N}). Figure 9(b) takes a different ‘slice’ of the non-rotating parameter space, where the static contact angle θ_A is fixed and one chooses the appropriate heating conditions (\hat{M}, \hat{N}) to attain bistability or completely coat the substrate (indefinite spreading).

Centrifugal forces tend to increase the size of the regions of bistability. For example, figure 10(a) exhibits regions of bistability for a completely wetting, $\theta_A = 0$, heated substrate, $\hat{M} > 0$, as it depends upon centrifugal number Ω^2 . Likewise, figure 10(b) illustrates that bistability can be achieved without heat transfer, $\hat{M} = 0$, if the substrate

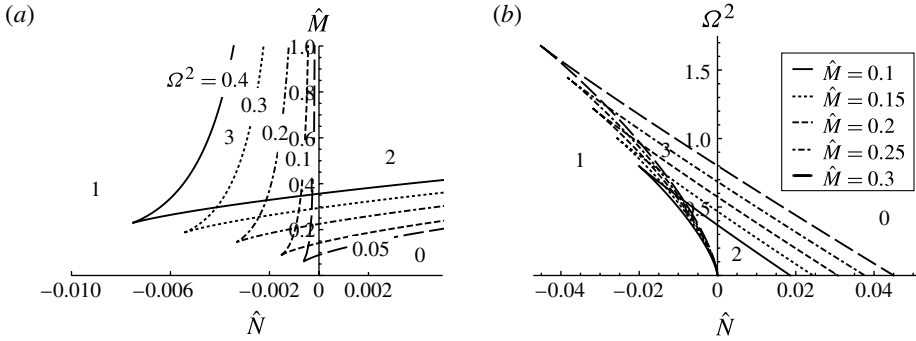


FIGURE 10. Parameter space for linear heating: vertical Marangoni number \hat{M} against radial Marangoni number \hat{N} , as it depends upon centrifugal number Ω^2 , for fixed static contact angle (a) $\theta_A = 0$ and (b) $\theta_A = 0.2$.

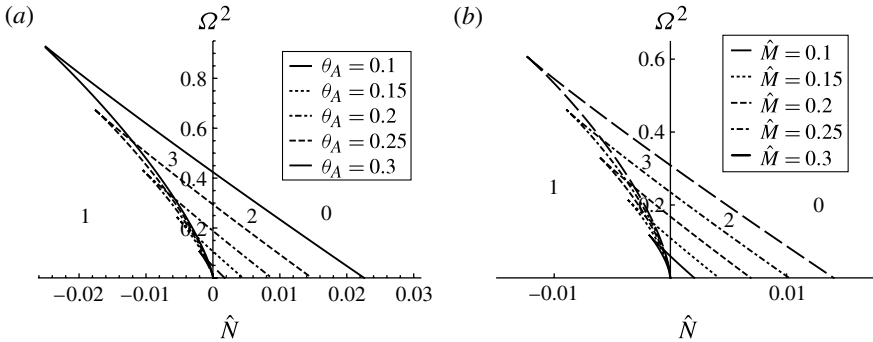


FIGURE 11. Parameter space for linear heating: centrifugal number Ω^2 against radial Marangoni number \hat{N} , as it depends upon (a) static contact angle θ_A ($\hat{M} = 0$) and (b) vertical Marangoni number \hat{M} ($\theta_A = 0$).

is partially wetting $\theta_A \neq 0$. Figure 11 shows the \hat{N} and Ω^2 parameter space for (a) thermally simple fluids $\hat{M} = 0$ and (b) completely wetting substrates $\theta_A = 0$.

4.4. Logarithmic heating

In this section, we analyse the applied temperature distribution with logarithmic profile (3.5). To avoid redundancy, results that are qualitatively similar to those of the previous section on linear heating will not be reproduced, such as bifurcation diagrams, flow fields, droplet shapes and the approach to equilibrium. Instead, we focus on the qualitative differences in the spreading regimes between linear and logarithmic heating conditions. The equilibrium contact-line radius a_∞ for logarithmic heating satisfies

$$C_{\hat{N}\Omega} a^3 - \hat{M} \left(\frac{3}{8} \right) a + \frac{4}{\pi a^3} - \theta_A = 0. \tag{4.2}$$

The biggest difference between linear (4.1) and logarithmic (4.2) heating is the lumped parameter $C_{\hat{N}\Omega}$ that represents the combined effect of a radial thermal gradient \hat{N} and centrifugal forces Ω^2 , which results in a reduction of independent system parameters

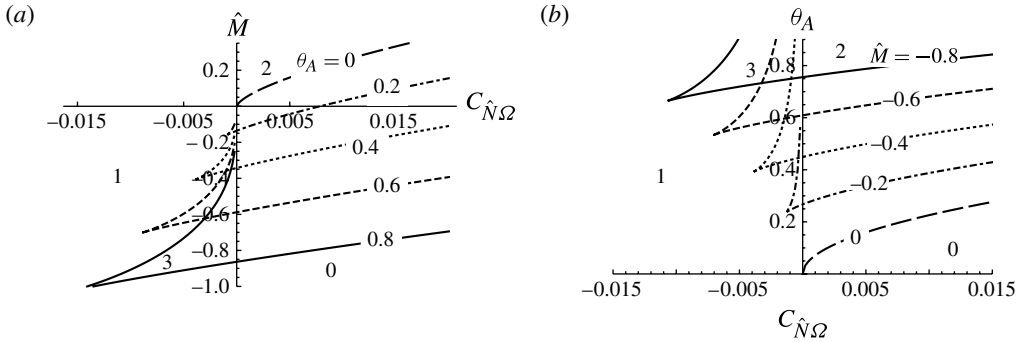


FIGURE 12. Parameter space for logarithmic heating: (a) vertical Marangoni number \hat{M} and (b) static contact angle θ_A against reduced parameter $C_{\hat{N}\Omega}$, as it depends upon (a) θ_A and (b) \hat{M} , respectively, to illustrate regions of bistability and indefinite spreading.

from four (linear) to three (logarithmic). This reduction results in a number of stronger restrictions on the system parameters to achieve bistability. In contrast to linear heating, conductive heat transfer ($\hat{M} < 0$) is a necessary condition to produce bistability for logarithmic heating (cf. figure 12). Figure 12 can be used as a guide in selecting spreading regimes to achieve a desired outcome, either bistability or indefinite spreading.

4.5. Comparison to experiments

In this section, we show that our results are qualitatively consistent with experiments by Mukhopadhyay & Behringer (2009). In particular Mukhopadhyay & Behringer (2009) show that a droplet on a completely wetting substrate ($\theta_A = 0$) can be made to retract to a smaller equilibrium radius by applying a radial temperature gradient directed from the contact line to the axis-of-symmetry ($\hat{N} < 0$). Recall that a drop spreading isothermally on a completely wetting substrate does not have an equilibrium radius and will spread indefinitely, as can be seen by setting $\hat{N} = \hat{M} = \Omega^2 = \theta_A = 0$ in (4.1). Our results demonstrate that there is an equilibrium configuration for $\hat{N} \neq 0$. For linear heating, we set $\hat{M} = \Omega^2 = \theta_A = 0$ in (4.1) and show that the equilibrium radius satisfies the following relationship:

$$\hat{N}a^7 = -\frac{32}{\pi^2}. \quad (4.3)$$

Note that the contact-line radius $a > 0$, so that there are only real equilibrium solutions for $\hat{N} < 0$, consistent with the experimental observation that a drop on a completely wetting substrate can be made to retract to a smaller equilibrium radius. We can derive a similar relationship for logarithmic heating by setting $\hat{M} = \Omega^2 = \theta_A = 0$ in (4.2) yielding

$$\hat{N}a^6 = -\frac{64}{3\pi^2}. \quad (4.4)$$

Once again, there are only real equilibrium solutions $a > 0$ when the radial thermal gradient is directed from the contact line to the axis-of-symmetry $\hat{N} < 0$.

The second observation made by Mukhopadhyay & Behringer (2009) is that the dynamics of the retraction process obey a characteristic power law. They use an

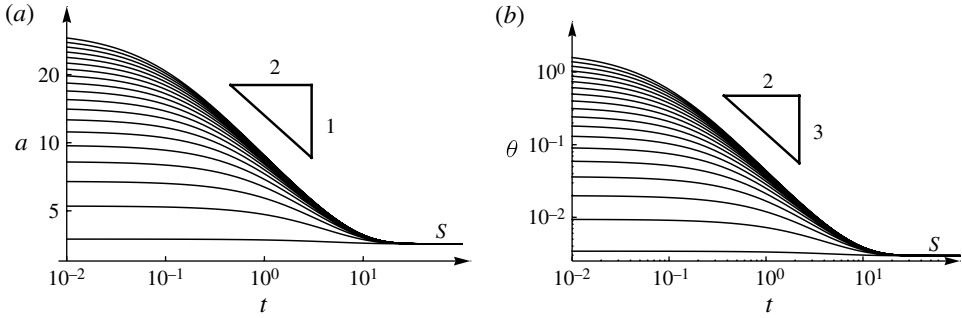


FIGURE 13. Time-dependent (a) contact-line radius and (b) contact angle computed from (3.7) for logarithmic heating on a completely wetting substrate $\theta_A = 0$ with spreading exponent $m = 1$, $\mathcal{K} = 1$ and $\hat{M} = \Omega^2 = 0$.

interferometric technique to measure the time-dependent contact angle throughout the retraction process. A least-squares fit of their data reveals that the contact angle behaves like a power law of the form $\theta \sim t^{-3/2}$. Our results recover this specific power law from the dynamic contact-line law (3.7) for logarithmic heating in the large-contact-line-radius limit $a \gg 1$. We set $\hat{M} = \Omega^2 = \theta_A = 0$, $\mathcal{K} = 1$, $m = 1$ and show that $da/dt \sim \hat{N}a^3$ for $a \gg 1$. When the thermal gradient is directed inwards $\hat{N} < 0$, $a \sim t^{-1/2}$ and $\theta \approx a^3 \sim t^{-3/2}$. We compare our asymptotic solution to the numerical solution of (3.7) in figure 13, which plots the time-dependent contact-line radius and contact angle for a droplet retracting on a completely wetting substrate. As shown, both the asymptotic and numerical solution yield a power law that matches experimental observations.

5. Concluding remarks

The spreading of an axisymmetric liquid drop on a smooth, non-uniformly heated solid substrate that is rotating at a constant angular velocity has been considered here. The lubrication approximation is applied to the field equations for this thin viscous fluid to generate an evolution equation for the interface shape, which is coupled to a dynamic contact-line condition that relates the contact angle to the contact-line speed. For small spreading rates, the droplet shape is steady and evolves implicitly through the time-dependent contact-line radius, which is governed by the dynamic contact-line law. In the absence of thermocapillary and centrifugal effects, droplet motion is driven by the imbalance of capillary (interfacial) and wetting (substrate) effects, and spreading proceeds until these effects are balanced. The manner in which thermocapillarity and centrifugal forces alter this balance is the focus of the present study.

We study the thermocapillary flows that result from the applied temperature distribution (radial gradient) and vertical heat transfer (vertical gradient). When the two thermocapillary effects interact, they can do so constructively or destructively. If the interaction is constructive, the thermocapillary flows can either assist or inhibit spreading and the droplet will spread indefinitely or converge to an equilibrium shape, which is uniquely determined by the thermal Marangoni numbers and wetting conditions on the solid substrate. If the thermocapillary flows interact destructively, bistability is possible. We show that in the absence of rotation $\Omega^2 = 0$, a droplet on

a partially wetting substrate ($\theta_A \neq 0$) exhibits bistability only when the applied radial gradient is directed inwards from the contact line to the axis-of-symmetry ($\hat{N} < 0$) while the drop is uniformly cooled, so that heat transfer is directed into the drop ($\hat{M} < 0$) (cf. figures 9 and 12). For the rotating geometry, we show that centrifugal forces enlarge the regions of bistability and relax the aforementioned restrictions on the heating conditions.

We have shown that our results for the logarithmic temperature profile are consistent with experimental observations made by Mukhopadhyay & Behringer (2009). Namely, we show that a drop on a completely wetting substrate can be made to retract to a smaller equilibrium radius by an applied thermal gradient and derive an expression relating the equilibrium radius to the magnitude of the thermal gradient. In addition, we use both an asymptotic and numerical solution to our governing equation to show that the dynamics of the retraction process obey a characteristic power law consistent with experimental observations.

Lastly, the majority of assumptions utilized here are reasonable when compared to typical experimental conditions and have been rationalized when first introduced. One exception is the assumption of small centrifugal number Ω^2 , which is meant to help clarify the results by illustrating the role centrifugal forces have in the spreading process. For example, one could argue that, in practice, centrifugal forces can be more easily controlled than conductive heat transfer across the drop interface. This suggests one should search for bistability in regions of parameter space where there is more control over experimental conditions. To extend this analysis to larger rotation rates, which are known to dewet (rupture) the centre of the droplet, one would need to include either a second contact line to model rupture or a disjoining pressure to prevent rupture. We also assume gravitational effects are negligible ($G = 0$), although they can become significant for large droplets on completely wetting surfaces. Finally, Mukhopadhyay *et al.* (2011) also report substrate temperature distributions localized near the contact line. Our model would need to be adapted to directly compare with such heating.

Acknowledgements

The author would like to thank M. Shearer, K. Daniels and J. Dijkstra for numerous helpful discussions regarding this work, as well as commenting on an earlier version of this manuscript. This work was supported by NSF grant no. DMS 0968258.

REFERENCES

- BENINTENDI, S. W. & SMITH, M. K. 1999 The spreading of a non-isothermal liquid droplet. *Phys. Fluids* **11**, 982–989.
- BONN, D., EGGERS, J., INDEKEU, J., MEUNIER, J. & ROLLEY, E. 2009 Wetting: statics and dynamics. *Rev. Mod. Phys.* **81**, 739–805.
- CHEN, C. D. 1988 Experiments on a spreading drop and its contact angle on a solid. *J. Colloid Interface Sci.* **122**, 60–72.
- CHEN, J. Z., TROIAN, S. M., DARHUBER, A. A. & WAGNER, S. 2005 Effect of contact angle hysteresis on thermocapillary droplet actuation. *J. Appl. Phys.* **97**, 014906.
- DANIEL, S., CHADHURY, M. K. & CHEN, J. C. 2001 Fast drop movements resulting from the phase change on a gradient surface. *Science* **291**, 633–636.
- DANIELS, K. E., BRAUSCH, O., PESCH, W. & BODENSCHATZ, E. 2008 Competition and bistability of ordered undulations and undulation chaos in inclined layer convection. *J. Fluid Mech.* **597**, 261–282.

- DARHUBER, A. A. & TROIAN, S. M. 2005 Principles of microfluidic actuation by modulation of surface stresses. *Annu. Rev. Fluid Mech.* **37**, 425–455.
- DARHUBER, A. A., TROIAN, S. M. & WAGNER, S. 2002 Generation of high-resolution surface temperature distributions. *J. Appl. Phys.* **91**, 5686–5693.
- DAVIS, S. H. 1987 Thermocapillary instabilities. *Annu. Rev. Fluid Mech.* **19**, 403–435.
- DUNN, G. J., DUFFY, B. R., WILSON, S. K. & HOLLAND, D. 2009 Quasi-steady spreading of a thin ridge of fluid with temperature-dependent surface tension on a heated or cooled substrate. *Q. J. Mech. Appl. Maths* **62**, 365–402.
- DUSSAN V., E. B. 1976 The moving contact line: the slip boundary condition. *J. Fluid Mech.* **77**, 665–684.
- DUSSAN V., E. B. 1979 On the spreading of liquid on solid surfaces: static and dynamic contact lines. *Annu. Rev. Fluid Mech.* **11**, 371–400.
- DUSSAN V., E. B. & DAVIS, S. H. 1974 On the motion of a fluid–fluid interface along a solid surface. *J. Fluid Mech.* **65**, 71–95.
- EHRHARD, P. 1993 Experiments on isothermal and non-isothermal spreading. *J. Fluid Mech.* **257**, 463–483.
- EHRHARD, P. 1994 The spreading of hanging drops. *J. Colloid Interface Sci.* **168**, 242–246.
- EHRHARD, P. & DAVIS, S. H. 1991 Non-isothermal spreading of liquid drops on horizontal plates. *J. Fluid Mech.* **229**, 365–388.
- FORD, M. L. & NADIM, A. 1994 Thermocapillary migration of an attached drop on a solid surface. *Phys. Fluids* **6**, 3183–3185.
- DE GENNES, P. G. 1985 Wetting: statics and dynamics. *Rev. Mod. Phys.* **57**, 827–863.
- GREENSPAN, H. P. 1978 On the motion of a small viscous droplet that wets a surface. *J. Fluid Mech.* **84**, 125–143.
- HOCKING, L. M. 1983 The spreading of a thin drop by gravity and capillarity. *Q. J. Mech. Appl. Maths* **36**, 55–69.
- HOCKING, L. M. 1992 Rival contact-angle models and the spreading of drops. *J. Fluid Mech.* **239**, 671–681.
- HUH, C. & SCRIVEN, L. E. 1971 Hydrodynamic model of steady movement of a solid/liquid/fluid contact line. *J. Colloid Interface Sci.* **35**, 85–101.
- LOPEZ, C. A. & HIRSA, A. H. 2008 Fast focusing using a pinned-contact liquid lens. *Nature Photonics* **2**, 610–613.
- MATAR, O. K. & CRASTER, R. V. 2009 Dynamics of surfactant-assisted spreading. *Soft Matt.* **5**, 3801–3809.
- MUKHOPADHYAY, S. & BEHRINGER, R. P. 2009 Wetting dynamics of thin liquid films and drops under marangoni and centrifugal forces. *J. Phys.: Condens. Matter* **21**, 464123.
- MUKHOPADHYAY, S., MURISIC, N., BEHRINGER, R. P. & KONDIC, L. 2011 Evolution of droplets of perfectly wetting liquid under the influence of thermocapillary forces. *Phys. Rev. E* **83**, 046302.
- NGUYEN, H. B. & CHEN, J. C. 2010a Numerical study of a droplet migration induced by combined thermocapillary-buoyancy convection. *Phys. Fluids* **22**, 122101.
- NGUYEN, H. B. & CHEN, J. C. 2010b A numerical study of thermocapillary migration of a small liquid droplet on a horizontal solid surface. *Phys. Fluids* **22**, 062102.
- ORON, A., DAVIS, S. H. & BANKOFF, S. G. 1997 Long-scale evolution of thin liquid films. *Rev. Mod. Phys.* **69**, 931–980.
- PEARSON, J. R. A. 1958 On convection cells induced by surface tension. *J. Fluid Mech.* **4**, 489–500.
- ROSENBLAT, S. & DAVIS, S. H. 1985 How do liquid drops spread on solids?. In *Frontiers in Fluid Mechanics* (ed. S. H. Davis & J. L. Lumley), pp. 171–183. Springer.
- SMITH, M. K. 1995 Thermocapillary migration of a two-dimensional liquid droplet on a solid surface. *J. Fluid Mech.* **294**, 209–230.
- SMITH, M. K. & DAVIS, S. H. 1983a Instabilities of dynamic thermocapillary liquid layers. Part 1. Convective instabilities. *J. Fluid Mech.* **132**, 119–144.
- SMITH, M. K. & DAVIS, S. H. 1983b Instabilities of dynamic thermocapillary liquid layers. Part 2. Surface-wave instabilities. *J. Fluid Mech.* **132**, 145–162.

- SPAID, M. A. & HOMSY, G. M. 1996 Stability of viscoelastic dynamic contact lines: an experimental study. *Phys. Fluids* **9**, 823–833.
- STONE, H. A., STROOCK, A. D. & AJDARI, A. 2004 Engineering flows in small devices: microfluidics toward a lab-on-a-chip. *Annu. Rev. Fluid Mech.* **36**, 381–411.
- TANNER, L. H. 1979 The spreading of silicone oil on horizontal surfaces. *J. Phys. D: Appl. Phys.* **12**, 1473.
- VOGEL, M., EHRHARD, P. & STEEN, P. 2005 The electroosmotic droplet switch: countering capillarity with electrokinetics. *Proc. Natl Acad. Sci.* **102**, 11974–11979.
- VOGEL, M. J. & STEEN, P. H. 2010 Capillarity-based switchable adhesion. *Proc. Natl Acad. Sci.* **107**, 3377–3381.
- ZIMMERMAN, D. S., TRIANA, S. A. & LATHROP, D. P. 2011 Bi-stability in turbulent, rotating spherical couette flow. *Phys. Fluids* **23**, 065104.